Ortega Pérez, M.; Juan Lizandra, MC.; Alcañiz Raya, ML.; Gil Gómez, JA.; Monserrat Aranda, C. (2008). Deformable brain atlas validation of the location of subthalamic nucleus using T1-weighted MR images of patients operated on for Parkinson's. Computerized Medical Imaging and Graphics. 32(5):367-378. doi:10.1016/j.compmedimag.2008.02.003

Deformable brain atlas. Validation of the location of Subthalamic Nucleus using T1-weightedMRImages of patients operated on for Parkinson's

M. Ortega, M. C. Juan, M. Alcañiz, J. A. Gil, C. Monserrat
Universitat Politècnica de València, Valencia, Spain

Abstract: Parkinson's disease is a degenerative disease of the central nervous system. One of the most effective treatments is deep brain stimulation. This technique requires the localization of an objective structure: the subthalamic nucleus. Unfortunately this structure is difficult to locate. In this work the creation of a deformable brain atlas that enables the identification of the subthalamic nucleus in T1-weighted Magnetic Resonance Imaging (MRI) in an automatic, precise and fast way is presented. The system has been validated using data from 10 patients (20 nucleus) operated on for Parkinson's. Our system offers better results using a Wendland function with an error of 1.8853±0.9959 mm.

Keywords: Brain atlas, Talairach-Tournoux, Elastic registration, Radial Basis Functions, Active Appearance Models, Subthalamic Nucleus, Parkinson's disease

1. Introduction

Parkinson's disease is a degenerative disease of the central nervous system characterized by a decrease in spontaneous movement, gait difficulty, postural instability, rigid-ity, and tremor. Frequently there are also other symptoms that develop as the disease advances (loss of intellectual capacity, psychological problems such as anxiety, depres-sion or isolation, small cramped handwriting, etc.) and moreover there is an increased risk of dementia and de-pression. This disease progresses inexorably towards dis-ability and death, and the rate of this progression is un-predictable. It is an important health issue that a ects al-most 2 out of every 100 people over the age of 64 years [1, 2]. Although the initial treatment for Parkinson's dis-ease is pharmacologic, in some cases this does not bring about adequate symptom control despite the diverse com-binations of medicines currently available. In other cases medication provokes disabling secondary e ects, like the appearance of abnormal movements or intolerance. These two situations occur more frequently as the period of treat-ment increases. A surgical intervention is recommended for these patients in order to control the Parkinson's symp-toms. There are other movement disorders (familiar essential trembling, post-traumatic trembling, etc.) that can also benefit from this surgical intervention. The disease is caused by degeneration of dopamine cells that in turn cause the nerve cells of the striatum to act without control, leav-ing the patient unable to direct or control their movements in a normal way. This degeneration takes place especially in the nigra substance and in the cells that project their axons towards the striatum (complex formed by the cauda-tum and putamen), associated with an hyperactivity of the inhibitory projections of the subthalamic nucleus (STN) that overstimulates the internal portion of globus pallidus (GPi) and the nigra substance (pars reticulata), that also inhibits the motor nucleus of the thalamus. This nucleus finally projects its axons towards the motor areas of the cerebral cortex, which are abnormally hyperexcited as a result of these alterations. For that reason, although there are experimental operations that attempt to repair lost neurons, the most used techniques attempt to remove the activity in the hyperactive nucleus (Vim, GPi or STN). During some time suppression was achieved by coagulating the nucleus, but it has been demonstrated that chronic stimulation with an alternating high frequency current is equivalent (deep brain stimulation). Deep brain stimulation is considered to have less complications and secondary effects, it is reversible, and its effect is more easily modulated [3, 4].

E-mail address: mcarmen@dsic.upv.es

1.1. *Problem of localizing the target*

The STN is a small lens-shaped nucleus in the brain, approximately 5.9 x 3.7 x 5 mm in size, where it is a part of the basal ganglia system. The STN is located ventral to the thalamus. It is also dorsal to the nigra substance and medial to the internal capsule. STN stimulation can exacerbate Parkinson's symptoms or can produce significant secondary effects. For this reason it is necessary to insert the electrode into the interior of the nucleus in a precise way. The STN is difficult to locate due to its small dimensions and anatomical characteristics. One of the ways to locate the STN is to use a stereotactical procedure, using an instrument that, fixed to the patient's skull, is able to locate three-dimensionally a reference brain, using a brain atlas. Brain atlases graphically represent different cerebral nuclei (among them the STN). In this way, it is possible to determine the distance of a certain nucleus (non-visible using radiological techniques) with respect to a visible reference (normally the line that joins the anterior commissure (AC) and posterior commissure (PC)). It is also possible to use statistical data from other patient interventions. Nevertheless the exact position of the STN in a certain patient does not necessarily have to agree with these data. This is due to individual anatomical variations between brains; this is the reason why it is necessary to confirm surgically that the STN has been reached or, on the contrary, to identify the structure that has been reached in order to relocate the electrode.

1.2. *Limitations of the surgical procedure*

The surgical procedure consists basically in:

- Locating the target using standard brain atlases.
- Registering a trajectory of about 15 to 20 mm with microelectrodes.
- Confirming the structures by means of this procedure with sensitive stimulation (driving) or macrostimulation.
- Choosing a new target using the data obtained.

Using this method, between 3 to 5 trajectories in each side are normally explored. Moreover the exploration for each stimulation has a duration of between 8 and 14 hours for each intervention. During this period of time, a displacement of the brain structures can occur, that will be greater depending on the time required for the intervention. This is due to the air intake through the burr hole, which can be minimized but is inavoidable [5]. Moreover, the risk of presenting complications (such as fundamental cerebral haemorrhage) is directly related to the duration of the intervention and the number of trajectories. On the other hand the patients are normally elderly with limitations to their functional capacity due to their disease and from whom medication has been withdrawn in order to better observe the effect during the intervention. For this reason they do not tolerate being immobilized for a long time well. Sometimes the procedure must be abandoned without obtaining the objective of the implant. The enormous complexity of this procedure, that requires the participation of a team of experts who use complex technology in long and expensive interventions, limits the possibility of offering this alternative treatment to all those who could potentially benefit from it. The procedure previously described can be highly optimized if the brain atlas is adjusted to the patients' anatomy.

1.3. *Related work*

In the last decade the number of publications related to deep brain stimulation has increased considerably [6]. In this paper, we only refer to techniques that are used to locate the STN. Slavin et al. [7] classify the methods used as direct or indirect. The indirect methods are based on the identification of the AC, PC and the use of brain atlases. The direct methods are based on the use of MRI images that allow us to visualize the STN. The type of MRI image commonly used to visualise the STN is the T2 type [7, 8, 9]. The STN is located in the lateral part of the red nucleus and dorsolateral of the nigra substance. These two anatomical structures are visible in T2-weighted MRI images (see Figure 1). T2 type MRI images are then merged with T1 type MRI images. Guo et al. [10] also presented a comparison between the different techniques that allows the location of the STN. They analyzed the following techniques:

(i) T2-weighted MRI-based targeting [7].

(ii) Anatomical brain atlas based targeting [11]. In this type of method brain atlases are used to identify the STN. Three of the most popular brain atlases are: Talairach-Tournoux [12], Schaltenbran-Wahren [13] and the probabilistic brain atlas of the Neurologic Institute of Montreal [14]. Most of these methods perform a non-rigid registration of the atlas in the MRI images [11, 15]. In the work of Guo et al. [10], an error of 3.2±1.1 mm was presented.

(iii) T1 and T2 map-based targeting [16, 17]. In this type of method, T2-type MRI images are used as an atlas. In these images the STN is identified and later the elastic adjustment with T1-type MRI images is made. Castro et al. [17] perform the non-rigid adjustment using different techniques: Affine registration, transformation of Schaltenbrand-Warhen, Demons algorithm and B-splines. They obtained best results using the B-splines with a mean error of 1.98±0.62 mm. They used 8 patients in the tests, and the patient in which the STN was better perceived was selected to be used as the atlas.

(iv) Electrophysiological database-based targeting [18]. This type of method stores and analyses data from surgical interventions. It is possible to obtain a standard template of the brain by normalising these data. In the end a probabilistic map of the population is

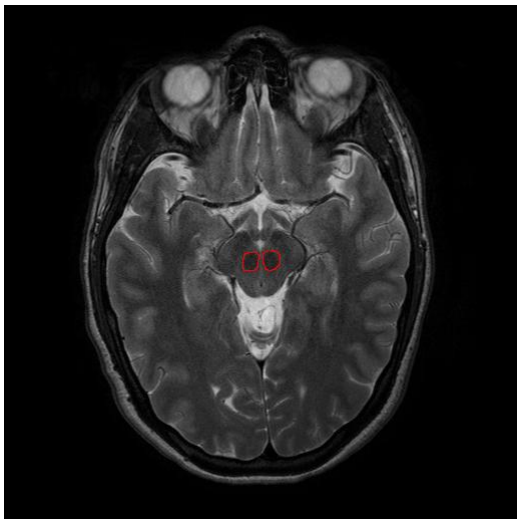

Fig. 1. Visualization of the red nucleus in T2-weighted MRI.

obtained that is based on data collected during the interventions in addition to its electrophysiological activity.

In Table 1, the results obtained with the different methods used by Guo et al. [10] are shown. They used the algorithm of Atamai-Warp [19] in order to obtain the non-rigid adjustment. Guo et al. [10] concluded that the best results are obtained when combining different techniques. In order to test the system they selected 10 patients from a database of 26 patients who had Parkinson's surgery.

2. Materials and methods

In order to locate the STN in MRI images of a patient, we have developed a deformable brain atlas based on the Talairach-Tournoux brain atlas. The tasks performed were as follows (see Figure 2):

- Transformation of MRI images of the patient in the coordinate system of Talairach.
- Segmentation of the homologous structures both in the atlas and in the MRI images of the patient's brain. In particular the cortex and ventricles in the MRI images are segmented using Active Appearance Models (AAMs) taking the axial slices of the Talairach's atlas as a reference.
- Non-rigid registration of the Talairach-Tournoux atlas in the MRI images using several Radial Basis Functions (RBF).
- Warp of the digital brain atlas over the MRI images.

2.1. *Talairach transform*

Using this transformation, the patient's brain has the same coordinate system as the Talairach-Tournoux brain atlas. This transformation is an affine transformation that works in parts. It uses different transformation matrices for each one of the 12 cubes that define the Talairach volume.

Several works have been based on this transformation, for example: Kruggel et al. [20] or Nowinski et al. [21]. This transformation presents several problems:

- The transformation is based on slices of a post mortem brain of a 60 year old woman who is not necessarily representative of the majority of the population.
- This transformation was developed for use in estereotactical procedures on the internal structures of the brain, not for the cortex.
- The spatial normalization based on AC and PC is not adequate for brain structures that represent greater variability. This variability increases with the respective distance from AC and PC.
- The transformation only allows linear transformations, that is: scale, rotations, translations.
- The transformation does not produce good results in brains that are affected by pathologies that produce deformations (e.g. tumours).

2.2. *Segmentation of structures in the Brain Atlas and in a patient's brain*

Once the brain is aligned in the coordinate system of Talairach, segmentation of the structures that will be used as homologues in our algorithm is performed. As has already been said, the cortex and ventricles in particular have been segmented both in the digital Talairach atlas and in MRI images of the patient. In order to achieve this, the method based on AAMs has been used.

The AAMs are statistical models that can represent variability both in form and in texture [22, 23] based on a training set. The training set consists of labelled images, where a set of key points are labelled in each object. The form of an object can be represented as vector η and the texture (level of greys) represented as vector g. The appearance model has c parameters that control the form and the texture:

$$\eta = \overline{\eta} + Q_s c \quad (1)$$

$$g = \overline{g} + Q_g c \quad (2)$$

Where η $\overline{\text{r}}$epresents the mean form, $\overline{g}$ the mean texture y Q_s, Q_g, are matrices that describe the manner of variation of the training set.

Using the Talairach-Tournoux atlas as a reference and 571 MRI images of different patients, 18 models were obtained. These models were initially trained by a neurosurgeon, using free tools available on Internet [23]. Several examples are shown in Figure 3. Table 2 presents all the information related to each model. AAMs have been used to locate different structures, for example: the mouth, face, eyes, etc. They have also been used for the segmentation of brain structures. Cootes et al.[23] performed segmentation of the ventricles, caudatum

Table 1
Locating Subthalamic Nucleus with the different methods used by Guo et al.

	Mean error (mm)	Max error (mm)	Min error (mm)	Standard Deviation (mm)
T2-weighted MRI	3.0	5.5	2.0	1.3
Brain atlas	3.2	6.2	2.1	1.1
T1 and T2 maps	2.9	5.7	2.2	1.1
EP database	2.7	5.8	1.8	1.2

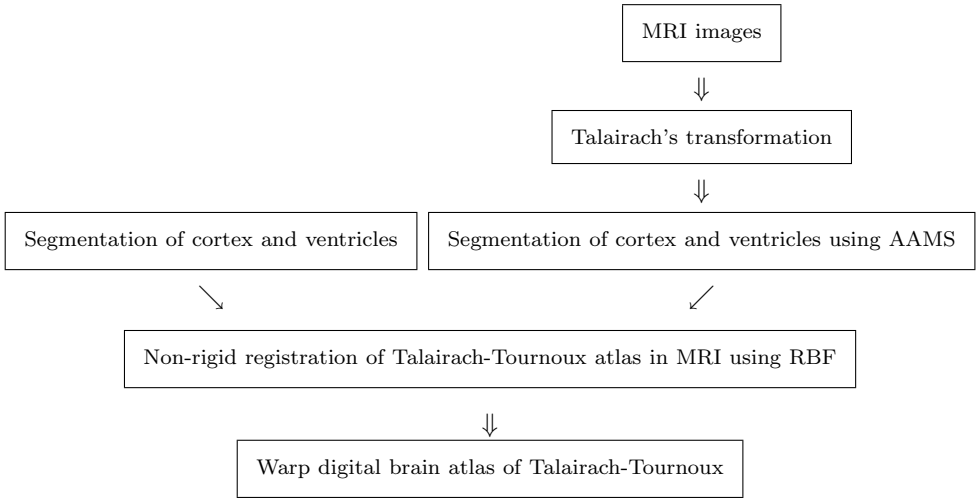

Fig. 2. Adjustment process.

nucleus and lentiform nucleus in 2D MRI images. However, as far as we know no previous research exists in which brain structures are segmented using AAMs based on the Talairach-Tournoux atlas.

The search performed by AAMs is an optimization problem where the difference between the synthesized object by the AAMs and the images has to be minimized. The difference vector is defined as:

$$\delta I = I_{image} - I_{model} \tag{3}$$

where I_{image} is the vector of grey levels in the image I_{model} is the vector of grey levels for the model parameters. Moreover, the optimization is sensitive to a good initialization. Cootes et al. [22] use a technique based on learning where AAMs are totally integrated and it is possible to adjust new images quickly using it. In order to evaluate the performance of the models two different approaches can be used [24]. The first of them consists in comparing the model with a ground truth, which is an image where key points have been identified by experts, or the same points used for the construction of the model can be used. The mean most used is the error point to curve or error of point associated to a curve (pt.crv). Defined as the Euclidean distance between a control point of the adjusted form in the new image, to the nearest point on the edge of the control points of the ground truth. The second approach consists in validating the result using the distribution of the training set, a property of the AAMs called self-contained validation that uses the error of texture between the image and the model. The mean $|\delta g|^2$. In our case we have used the first approach and the results are presented in Table 2. In Table 2 it is possible to observe the error pt.curve for each model. Figure 3 (d) presents the results of the search using different models in different MRI images.

2.3. *Non rigid registration using RBF with compact support*

One of the best-known non-rigid methods is the use of RBF. The use of RBF in the medical image adjustment problem was originally introduced by Bookstein [25]. Bookstein studied deformation in images of patients a ected by Apert Syndrome. Apert Syndrome is characterized by the premature closing of the skull sutures, which causes the head to take a pointed form and the deformation of the face. The RBF method is based on the use of control points, so that if we identify a series of control points in both images (volumes), ensuring that these points are homologous, the problem is to determine the transformation function that allows the identification of any point between both images (volumes). In our case the initial volume is the digitized atlas of Talairach-Tournoux and the destination volume is the MRI of the patient. This problem is equivalent to solve a problem of interpolation:

$$X = \{(x_i, y_i, z_i)\}_{i=1}^{N} \in \Omega \subseteq \mathbb{R}^3 \quad \text{(atlas landmarks)} \tag{4}$$

$$Y = \{(u_i, v_i, w_i)\}_{i=1}^{N} \in \Delta \subseteq \mathbb{R}^3 \quad \text{(MRI landmarks)} \tag{5}$$

$T(x, y, z) \in C^{k \geq 0}$ is wanted to determine with components $T_x(x, y, z)$, $T_y(x, y, z)$ and $T_z(x, y, z)$ that fulfills::

Table 2
Information about the AAMs based on the Talairach's atlas slices

Model	Distance (mm) ±2 mm	Training images	Used points		Pt. crv (Mean)	Pt. crv (S.D)	Pt. crv (Median)
			Ventricles	Cortex			
A	+60	41	—	99	1.99	0.46	0.98
B-C	+50	35	—	100	1.86	0.55	0.75
D-E-F	+40	49	—	104	1.51	0.31	0.89
G-H-I	+35	36	—	100	0.81	0.07	0.67
J	+24	27	24	89	2.28	0.54	0.86
K	+20	36	45	89	0.92	0.22	0.51
L	+16	34	59	121	1.48	0.41	1.37
M-N	+10	26	80	121	0.80	0.19	0.42
O	+4	24	109	141	1.68	0.35	0.65
P	+1	28	86	137	1.36	0.35	1.03
Q	-1	26	70	143	0.99	0.37	0.46
R	-4	25	48	142	1.08	0.31	0.62
S	-8	24	35	122	0.92	0.13	0.55
T	-12	43	24	74	1.70	0.34	0.74
U	-16	12	12	46	1.26	0.21	1.00
V	-20	22	—	32	4.46	1.12	1.16
W-X	-26	36	—	28	6.45	1.08	3.00

$$u_i = T_x(x_i, y_i, z_i), \quad i = 1 \ldots, N \tag{6}$$
$$v_i = T_y(x_i, y_i, z_i), \quad i = 1 \ldots, N \tag{7}$$
$$w_i = T_z(x_i, y_i, z_i), \quad i = 1 \ldots, N \tag{8}$$

The interpolation problem will be solved separately for each coordinate. In this case $T_x(x, y, z)$ indicates the displacement of variable x, $T_y(x, y, z)$ indicates the displacement of variable y, and $T_z(x, y, z)$ indicates the displacement of variable z.

Therefore, if we use RBF to solve the problem we will have an interpolation function with the following form:

$$\zeta_x(x, y, z) = \beta_{1,z} + \beta_{2,z}x + \beta_{3,z}y + \beta_{4,z}z \tag{9}$$
$$\zeta_y(x, y, z) = \beta_{1,y} + \beta_{2,y}x + \beta_{3,y}y + \beta_{4,y}z \tag{10}$$
$$\zeta_z(x, y, z) = \beta_{1,z} + \beta_{2,z}x + \beta_{3,z}y + \beta_{4,z}z \tag{11}$$

$$T_x(x, y, z) = \zeta_x(x, y, z) + \sum_{j=1}^{N} \alpha_{j,x}\psi(\|(x, y, z) - (x_j, y_j, z_j)\|)$$

$$T_y(x, y, z) = \zeta_y(x, y, z) + \sum_{j=1}^{N} \alpha_{j,y}\psi(\|(x, y, z) - (x_j, y_j, z_j)\|)$$

$$T_z(x, y, z) = \zeta_z(x, y, z) + \sum_{j=1}^{N} \alpha_{j,z}\psi(\|(x, y, z) - (x_j, y_j, z_j)\|)$$

If we impose the interpolation conditions:

$$T_x(x_i, y_i, z_i) = u_i \quad i = 1, \ldots, N \tag{12}$$
$$T_y(x_i, y_i, z_i) = v_i \quad i = 1, \ldots, N \tag{13}$$
$$T_z(x_i, y_i, z_i) = w_i \quad i = 1, \ldots, N \tag{14}$$

we have to add the conditions of orthogonality in order to guarantee that the interpolation problem is condition number [26, 27], therefore, these orthogonality conditions will be:

$$\sum_{i=1}^{N} \alpha_{i,x} = 0 \qquad \sum_{i=1}^{N} \alpha_{i,y} = 0 \qquad \sum_{i=1}^{N} \alpha_{i,z} = 0 \tag{15}$$
$$\sum_{i=1}^{N} \alpha_{i,x}x_i = 0 \qquad \sum_{i=1}^{N} \alpha_{i,y}x_i = 0 \qquad \sum_{i=1}^{N} \alpha_{i,z}x_i = 0 \tag{16}$$
$$\sum_{i=1}^{N} \alpha_{i,x}y_i = 0 \qquad \sum_{i=1}^{N} \alpha_{i,y}y_i = 0 \qquad \sum_{i=1}^{N} \alpha_{i,z}y_i = 0 \tag{17}$$
$$\sum_{i=1}^{N} \alpha_{i,x}z_i = 0 \qquad \sum_{i=1}^{N} \alpha_{i,y}z_i = 0 \qquad \sum_{i=1}^{N} \alpha_{i,z}z_i = 0 \tag{18}$$

From here it is possible to deduce the following equation system:

$$Aw = B \tag{19}$$

that is a linear equation system with 3 independent terms, where A is a real and symmetric matrix. Once the equation system is solved, the $3(N + 4)$ coefficients of the function will have been determined: 12 for the polynomial part, and $3N$ for the radial part.

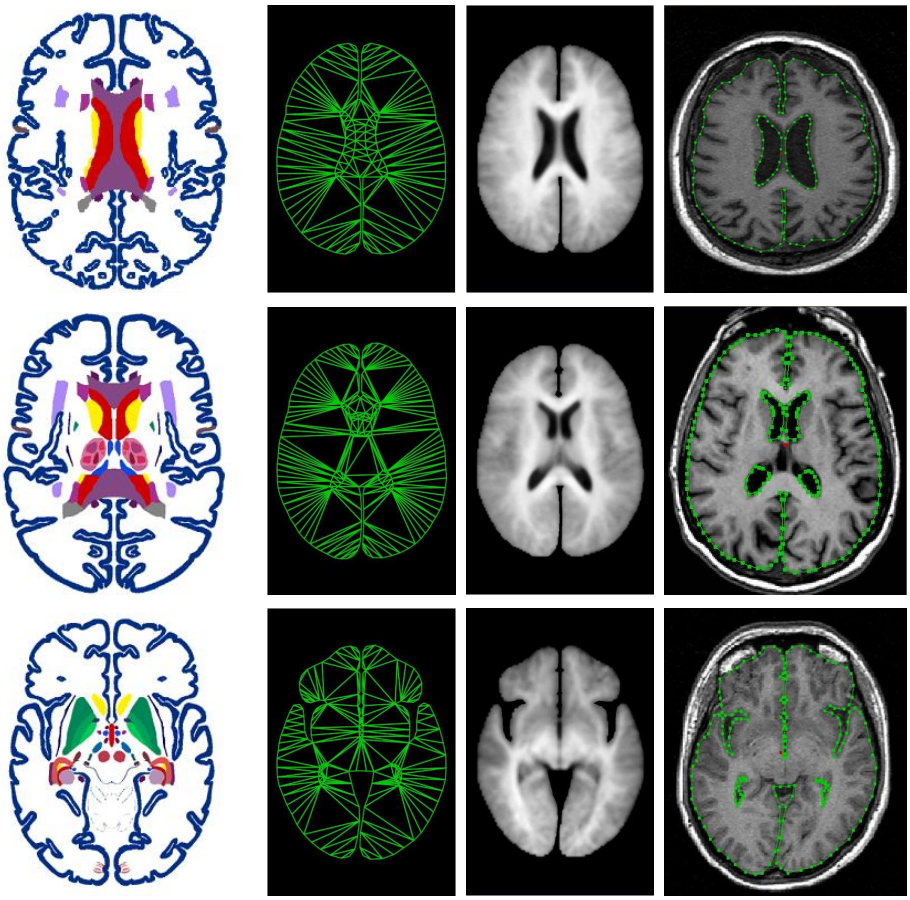

Fig. 3. Examples of AAMs and their application to MRI images: (a) Original slices of the Talairach-Tournoux atlas; (b) Mean model of texture; (c) Mean model of form; (d) Segmentation of cortex and ventricles using (b) model.

If we call

$$A = \begin{bmatrix} K & P \\ P^T & O \end{bmatrix} \quad \in Mat((N+4)\times(N+4)) \tag{20}$$

and we developed it in more detail, we have

$$A = \left[\begin{array}{cccc|cccc} r_{1,1} & r_{1,2} & \dots & r_{1,N} & 1 & x_1 & y_1 & z_1 \\ r_{2,1} & r_{2,2} & \dots & r_{2,N} & 1 & x_2 & y_2 & z_2 \\ \vdots & \vdots & \ddots & \vdots & \vdots & \vdots & \vdots & \vdots \\ r_{N,1} & r_{N,2} & \dots & r_{N,N} & 1 & x_N & y_N & z_N \\ \hline 1 & 1 & \dots & 1 & 0 & 0 & 0 & 0 \\ x_1 & x_2 & \dots & x_N & 0 & 0 & 0 & 0 \\ y_1 & y_2 & \dots & y_N & 0 & 0 & 0 & 0 \\ z_1 & z_2 & \dots & z_N & 0 & 0 & 0 & 0 \end{array}\right] \tag{21}$$

where $r_{i,j} = \psi(||(x_i - x_j, y_i - y_j, z_i - z_j)||)$.

From the matrices it is possible to deduce that A matrix is symmetric. The matrix of independent terms and the matrix of unknown factors are the following:

$$B = \begin{bmatrix} u_1 & v_1 & w_1 \\ u_2 & v_2 & w_2 \\ \vdots & \vdots & \vdots \\ u_n & v_n & w_n \\ 0 & 0 & 0 \\ 0 & 0 & 0 \\ 0 & 0 & 0 \\ 0 & 0 & 0 \end{bmatrix} \quad \omega = \begin{bmatrix} \alpha_{x,1} & \alpha_{y,1} & \alpha_{z,1} \\ \alpha_{x,2} & \alpha_{y,2} & \alpha_{z,2} \\ \vdots & \vdots & \vdots \\ \alpha_{x,n} & \alpha_{y,n} & \alpha_{z,n} \\ \beta_{x,1} & \beta_{y,1} & \beta_{z,1} \\ \beta_{x,2} & \beta_{y,2} & \beta_{z,2} \\ \beta_{x,3} & \beta_{y,3} & \beta_{z,3} \\ \beta_{x,4} & \beta_{y,4} & \beta_{z,4} \end{bmatrix} \tag{22}$$

In order to solve the interpolation problem the following RBF are usually used:

- Thin plate spline: $\psi(r) = r$.
- Multiquadratic: $\psi(r) = \sqrt{c^2 + r^2}$, where $c \neq 0$ is a free selection parameter.
- $\psi(r) = e^{-cr^2}$ where $c > 0$ is a parameter.

We have guaranteed the solution of the equation sys-

tem (19) for the RBF previously described [27, 28]. In the present research we will use the Thin Plate Spline and the family of functions of Wendland and Wu.

2.4. *Wendland and Wu functions*

Two important classes of RBF with compact support are the families of functions of Wu [29] and Wendland [26]. These functions are polynomials and positive-defined. For a certain dimension $d > 0$ and a smoothness parameter $k \geq 0$ a unique Wendland function exists:

$$\psi_{d,k} := I^k(1-r)_+^{\lfloor d/2 \rfloor + k + 1}(r) \in C^{2k}(\mathbb{R}) \tag{23}$$

where

$$f_d(r) = (1-r^2)_+^l = \begin{cases} (1-r^2)^l, & \text{if } 0 \leq r \leq 1; \\ 0, & \text{otherwise.} \end{cases} \tag{24}$$

and $I\psi(r) := \int_r^\infty t\psi(t)dt \quad r \geq 0$ is the integral operator. This function is positive-defined in $\mathbb{R}$ and polynomial whose minimum degree is floor(d/2)+3k+1. Let's look at some of these functions:

- $\psi_{3,0} = (1-r)_+^2 \in C^0(\mathbb{R})$ WEN0.
- $\psi_{3,1} = (1-r)_+^4(4r+1) \in C^2(\mathbb{R})$ WEN1.
- $\psi_{3,2} = (1-r)_+^6(35r^2+18r+3) \in C^4(\mathbb{R})$ WEN2.

Respect to Wu uses the function (24) and by means of the convolution operator $*$ constructs $\phi_{d,0}(r) = (f_d * f_d)(r)$ then $\phi_{d,k} = D^k\phi_{d,0}(r)$ is defined, where $D = \frac{-1}{r}\frac{d}{dr}$ is the differential operator. $\phi_{d,k}$ is positive-defined in $\mathbb{R}^d$ for $d \leq 2k+1$ and polynomial of degree $4l-2k+1$ in the interior of the support.

Some examples of Wu functions for $d = 3$ are:

- $\phi_{3,1} = (1-r)_+^6(5r^5+30r^4+72r^3+82r^2+40r+8) \in C^4(\mathbb{R})$ WU1.
- $\phi_{3,2} = (1-r)_+^5(5r^4+25r^3+48r^2+40r+8) \in C^2(\mathbb{R})$ WU2.
- $\phi_{3,3} = (1-r)_+^4(5r^3+20r^2+29r+16) \in C^0(\mathbb{R})$ WU3.

As Wu and Wendland functions are positive-defined [26], the resolution of the equation system (19) is guaranteed. These functions can be scaled by a parameter $\mu > 0$ so that,$\psi_{d,k,\mu}(r) \equiv \psi_{d,k,\mu}(r/\mu)$ (same argument is valid for the Wu functions) and so their mathematic properties are not affected, with this the size of the support is changed from [0,1] to $[0,\mu]$. Changing the size of the support means that the elastic transformation will be limited to the points of the volume that are within the support.

2.5. *RBF properties*

In this section some properties of the RBF are cited:

- Nature of the transformation. In the case of the RBF the polynomial part is in charge of performing an affine transformation, whereas the radial part is in charge of performing the elastic transformation.
- Locality of the transformation. The locality determines the spatial range where the transformation has influence, that is, if the transformation affects the whole image or only a certain area of the image. The election of the RBF is determinant because it affects locality, since, depending on the RBF used the transformation will be global and/or local.
- Computational cost. As in previous sections the selection of the RBF will be the determinant for the computational cost. RBF with compact support will offer computational advantages, since the matrix is dispersed. When increasing the size of the support, the matrices will become more and more dense. This will allow us to use iterative methods of resolution. On the other hand if we used another type of RBF like the Thin Plate Spline the matrix will be completely dense.
- Stability. In general, the matrices resulting from the problem (19) are usually very badly conditioned. This is not the case of the RBF with compact support since, in general, they are usually well conditioned, increasing the number of the matrix condition as the support size increases.
- Differentiability. The analysis of the differentiability will be determinant in RBF with compact support, because this factor will change the results of the adjustment enormously.

3. Results

In order to validate our method, we have used data from 10 patients (20 nucleus) operated on for Parkinson's, in which the location of the STN was identified as the final position of the microelectrodes. This position was compared with the one obtained by our method. In order to achieve this, the mean quadratic error between the position obtained by our method and the final position of the microelectrode was calculated. The MRI images have a distance between pixels in x and y of 0.859375 mm and the distance between the slices is 1 mm. The equipment used to take these images is: Philips Gyrosxcan ACS-NT (Best, Holland) equipped with a superconducting magnet of 1.5 Teslas and field gradients of 15 field of mT/m.

3.1. *2D Test*

In this section 2D visual results are presented. Figure 4 shows the result of the Wu function of class 0 (WU3) with support size $\lambda = 41$. The axial slice of the atlas is the number 10, at +20 mm. This figure shows visually how accurate the adjustment of the brain atlas to a patient's brain is.

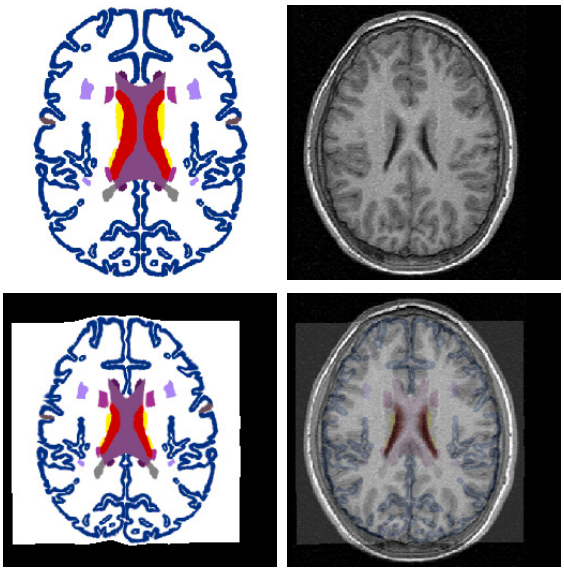

Fig. 4. Example of Talairach's atlas adjustment.

3.2. *Accuracy*

In order to validate the quality of the adjustment, several RBF were used, specifically the RBF of Wendland, Wu and the Thin Plate Spline. We have checked how the size of the support and the smoothness a ect the results of the adjustment when using RBF with compact support. Figures 5 and 6 present the results (mean error and stan-dard deviation) using our method for locating the STN (left + right) in 10 patients.

Among the RBF used, the one that gave the best results was the Wendland function of:$\psi_{3,0}(r) = (1-r)^2_+$ with a support size of $\lambda = 34$ with an error of 1.8853±0.9959 mm, followed by the Wu function: $\phi_{3,3}(r) = (1-r)^4_+(5r^3 + 20r^2 + 29r + 16)$ with a support size of $\lambda = 24$ with an error of 2.0129±1.0356 mm. The other RBF have given worse results. Moreover, it can be seen that increasing the smoothness of the RBF with support gave worse results.

We can compare our results with previous results from two points of view:

– Methods that are based on digital brain atlases. Ganser et al. [11] used a brain atlas (Talairach) and RBF. The best results were reported using the Wendland function, as in our case. They obtained the distance to the frontal end of the putamen (left-right) using Wendland function and Thin Plate Spline. The errors are: Thin Plate Spline, left: 5.61±1.93, right: 5.89±2.90; Wendland function, left: 4.76±2.03, right: 3.99±1.76. Guo et al. [10] reported an error of 3.2±1.1 mm. Our method gives better result than these two works.
– Methods that use RBF. Castro et al. [17] uses a T2-weighted MRI as an atlas and performs the non-rigid adjustment using different techniques, among them B-splines which offered better results, with a mean error of 1.98±0.62 mm. Our error is a bit lower that this error.

Table 3
Number of non-null elements of matrix A and condition number

	Non-null elements	Memory (megas)	Condition number
$\psi_{3,0,1}$	24649	0.1462	$1.0935{\cdot}10^4$
$\psi_{3,0,15}$	99707	0.7575	$1.4634{\cdot}10^4$
$\psi_{3,0,30}$	330643	1.8972	$2.9279{\cdot}10^5$
$\psi_{3,0,45}$	705933	4.0446	$4.3965{\cdot}10^5$
$\psi_{3,0,50}$	866435	4.9630	$4.8873{\cdot}10^5$
$\psi_{3,0,70}$	1725737	9.8800	$6.8579{\cdot}10^5$
TPS	7510328	28.6496	$1.3232{\cdot}10^7$

3.3. *Computational cost*

In this section we will concentrate on the following aspects:

(i) Construction of the equation system.
(ii) Resolution of the equation system.
(iii) Evaluation of the transformation function.

Storage cost

If RBF with compact support are used, the matrix of system A is dispersed. This is because these functions are the product of the function (24) by a polynom, and this function is null in the points that are inside the support. The degree of dispersion of the matrix will depend, to a great extent, on two factors:

– Support size.
– Distribution of the control points.

The number of elements affected by the transformation increases when the support size is increased, therefore, the number of non-null elements of matrix A will be increased. On the contrary if the Thin Plate Spline is used, the matrix of the system is dense since the transformation affects all the control points of the image. Both in the Thin Plate Spline and RBF with compact support the matrix of the system is symmetric, therefore it will only be necessary to store half of the matrix elements. Moreover in the case of the RBF with compact support, this cost can be reduced in $O(N)$ using the technique described by Morse et al. [28].

Table 3 shows different examples where the number of non-null elements of the system A matrix using several RBF appear. More specifically, 2837 points in the cortex and ventricles were identified in order to perform non-rigid registration between the Talairach's atlas and the MRI images of the patient. Figure 7 shows the matrix dispersion using different RBF.

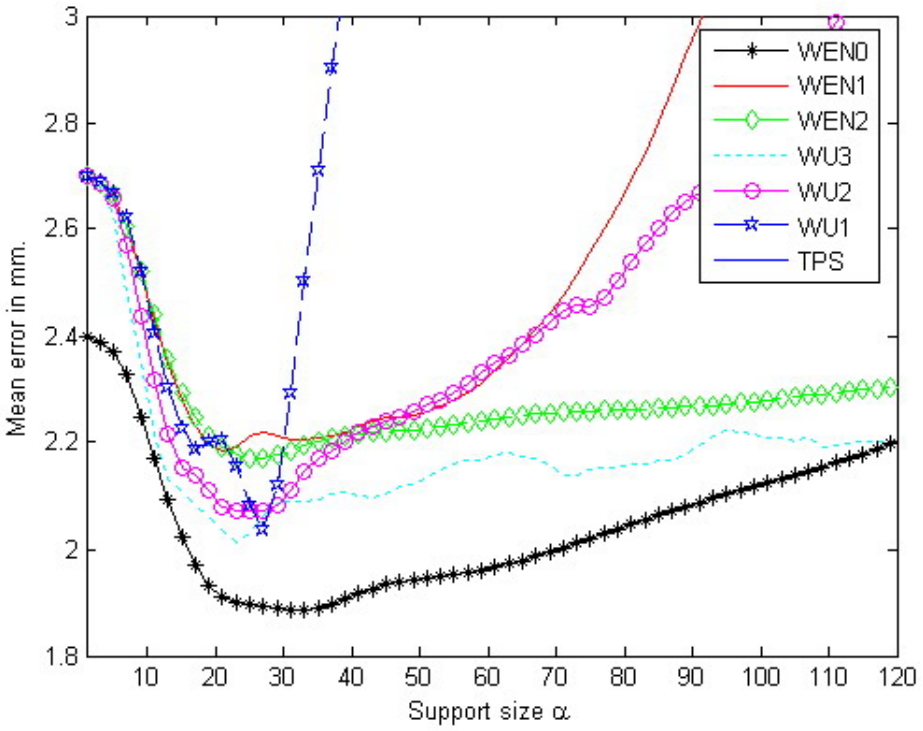

Fig. 5. Mean error (STN left+right) in mm. changing support size.

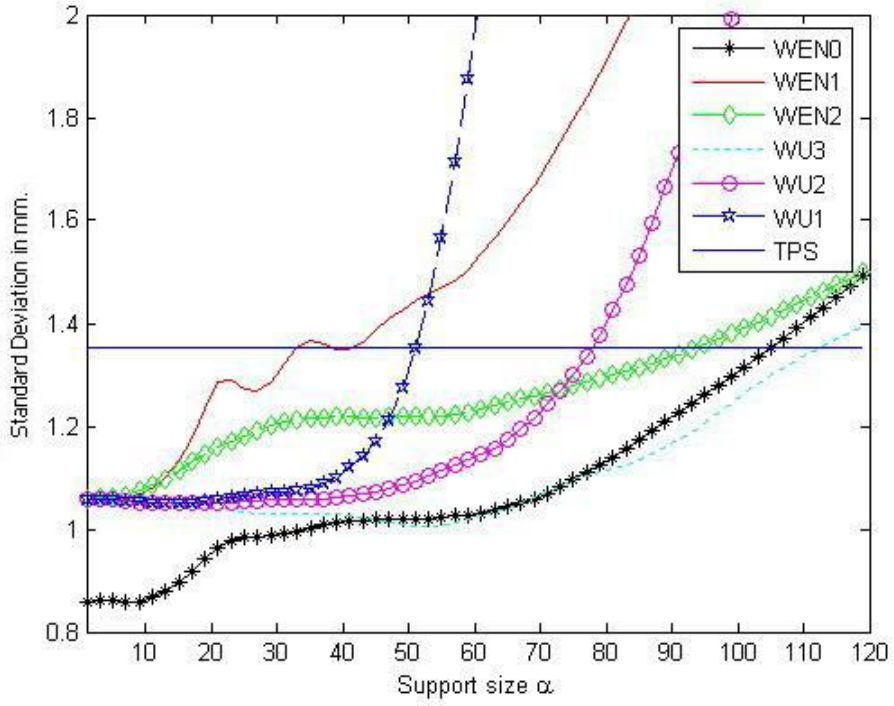

Fig. 6. Standard deviation (STN left+right) in mm. changing support size.

Table 4
Computational cost TPS vs RBF with compact support

	TPS	CSRBFs
Computation to build	$O(N^2)$	$O(N \log N)$
Computation to solve	$O(N^2)$	$O(N^{1.5})$
Storage to build/solve	$O(N^2)$	$O(N)$
Computation to evaluate	$O(N)$	$O(\log N)$

Solving the equation system

The resolution of the equation system (19) using LU decomposition is an operation of $O(N^3)$. The computational cost can be reduced to an operation of $O(N^2)$ using iterative methods (method of the biconjugated gradients). On the other hand if we used RBF with compact support, and the mean number of control points inside the support size for each (x_i, y_i, z_i) is less than a constant ϵ, this implies that the number of non-null entries of the matrix A is $O(N)$. In this case a LU decomposition for dispersed matrices would be used in order to find the solution of the equation system [30]. The order of this method varies from $O(N^{1.2})$ to $O(N^{1.5})$ depending on the "fill in" produced during the decomposition. Table 4 presents the computational cost of the Thin Plate Spline and RBF with compact support.

With respect to the stability of the equation system (19), in the case of the RBF with compact support the system matrix is usually well conditioned. The number of condition will be depend on 3 factors:
– The number of points.
– Distribution of points.
– Support size.
One way to know if points are well distributed is to calculate the separation distance:

$$\eta = \frac{1}{2} \min_{1 \le j \ne i \le N} ||(x_j, y_j, z_j) - (x_i, y_i, z_i)|| \qquad (25)$$

Table 3 shows different examples where the number of condition of the matrix A using several RBF appears.

Evaluating the transformation function

To evaluate the interpolation function of the Thin Plate Spline is an operation of $O(N)$. This time can be reduced in RBF with compact support using "k-tree" method to an operation of $O(\log N)$.

Implementation

The resolution of the equation system was performed using CLAPACK library [31]. Table 5 shows the time in seconds needed to solve the system. The computer used was a Pentium IV 1.4 Ghz. The function evaluated was WEN0 with a support size of 35.

4. Discussion

In this research a deformable brain atlas that allows the location of different anatomical structures in patients' brains has been developed. We have applied it to the location of the STN. It has been demonstrated that RBF, especially those with compact support, are effective methods for elastic adjustment, both in terms of computational cost and the accuracy of the adjustment. Among all RBF used the one that has given the best results is the Wendland function: $\psi_{3,0}(r) = (1-r)_+^2$ with a support size of $\lambda = 35$, followed by the Wu function: $\phi_{3,3}(r) = (1-r)_+^4(5r^3 + 20r^2 + 29r + 16)$ with a support size of 24. The rest of the functions have given worse results. Our results have been compared with results given in other works and ours are more accurate.

As to future research, we want to establish formal cri-

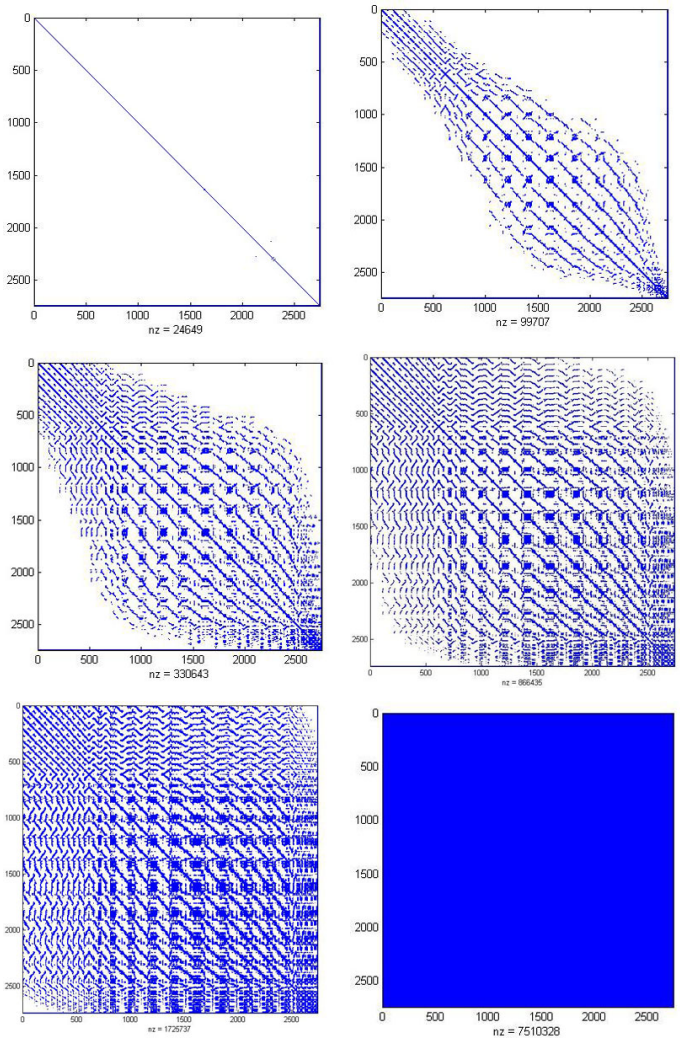

Fig. 7. Matrix dispersion using different RBF.

Table 5
Time required for solving the equation system (19)

	Number of points	Time (in seconds)
2D	241	0.3
3D	2837	30

teria to select the support size, to incorporate elasticity properties of the materials into our model, to increase the number of images of the AAMs and to apply the model in the identification of new anatomical structures.

5. Summary

Parkinson's disease is a degenerative disease of the central nervous system characterized by a decrease in spontaneous movement, gait difficulty, postural instability, rigidity, and tremor. Nowadays, one of the most effective treatments is deep brain stimulation. This technique requires the localization of an objective structure: the subthalamic nucleus. Unfortunately this structure is difficult to locate using traditional techniques due to its small dimensions and anatomical characteristics. In this work the creation of a deformable brain atlas that enables the iden-tification of the subthalamic nucleus in T1-weighted magnetic resonance imaging (MRI) in an automatic, precise and fast way is presented. The Talairach-Tournoux brain atlas has been used. The method consisted of: (i) the location of the MRI images in Talairach's coordinate system; ii) the identification of homologous structures (cortex and ventricles) between the brain atlas and the MRI images using Active Appearance Models (AAMs) based on the 27 axial slices of the Talairach's atlas; (iii) Non-rigid registra-tion between the atlas of Talairach-Tournoux and the MRI images using several Radial Basis Functions (RBF), among them different Radial Basis Functions with compact support. The system has been validated using data from 10 patients (20 nucleus) operated on for Parkinson's, in which the final placement of the microelectrode was considered the correct placement for the subthalamic nucleus. This placement was compared with the one obtained using our method. In order to achieve this, the mean squared error between the position of the subthalamic nucleus obtained by our method and the final position of the microelectrodes was calculated. Our system offers better results using a Wendland function with an error of 1.8853±0.9959 mm.

References

[1] S. Campenhausen, B. Bornschein, R. Wick, K. Btzel, C. Sampaio, W. Poewe, W. Oertel, U. Siebert, K. Berger, and R. Dodel. Prevalence and incidence of parkinson's disease in europe. *Eur Neuropsychopharmacol*, 15(4):473–490, Aug 2005.

[2] E. D. Louis, K. Marder, L. Cote, M. Tang, and R. Mayeux. Mortality from parkinson disease. *Arch Neurol*, 54(3):260–264, Mar 1997.

[3] Y. Katayama, H. Oshima, T. Kano, K. Kobayashi, C. Fukaya, and T. Yamamoto. Direct effect of subthalamic nucleus stimulation on levodopa-induced peak-dose dyskinesia in patients with parkinson's disease. *Stereotact Funct Neurosurg*, 84(4):176–179, Aug 2006.

[4] J. A. Obeso, M. C. Rodriguez-Oroz, M. Rodriguez, R. Macias, L. Alvarez, J. Guridi, J. Vitek, and M. R. DeLong. Pathophysiologic basis of surgery for parkinson's disease. *Neurology*, 55(12):S7–12, 2000.

[5] X. Morandi, C. Haegelen, P. Henaux, and L. Riffaud. Brain shift is central to the pathogenesis of intracerebral haemorrhage remote from the site of the initial neurosurgical procedure. *Med Hypotheses*, 67(4):856–859, 2006.

[6] Clement Hamani, Erich Richter, Jason M Schwalb, and Andres M Lozano. Bilateral subthalamic nucleus stimulation for parkinson's disease: a systematic review of the clinical literature. *Neurosurgery*, 56(6):1313–21; discussion 1321–4, Jun 2005.

[7] K. V. Slavin, K. R. Thulborn, C. Wess, and H. Nersesyan. Direct visualization of the human subthalamic nucleus with 3t mr imaging. *AJNR Am J Neuroradiol*, 27(1):80–84, Jan 2006.

[8] Nikunj K Patel, Peter Heywood, Karen O'Sullivan, Seth Love, and Steven S Gill. Mri-directed subthalamic nucleus surgery for parkinson's disease. *Stereotact Funct Neurosurg*, 78(3-4):132–145, 2002.

[9] M. Egidi, P. Rampini, M. Locatelli, M. Farabola, A. Priori, A. Pesenti, F. Tamma, E. Caputo, V. Chiesa, and R. M. Villani. Visualisation of the subthalamic nucleus: a multiple sequential image fusion (musif) technique for direct stereotaxic localisation and postoperative control. *Neurol Sci*, 23 Suppl 2:S71–S72, Sep 2002.

[10] T. Guo, K. W. Finnis, S. C. L. Deoni, A. G. Parrent, and T. M. Peters. Comparison of different targeting methods for subthalamic nucleus deep brain stimulation. In *MICCAI (1)*, pages 768–775, 2006.

[11] Klaus A Ganser, Hartmut Dickhaus, Roland Metzner, and Christian R Wirtz. A deformable digital brain atlas system according to talairach and tournoux. *Med Image Anal*, 8(1):3–22, Mar 2004.

[12] J. Talairach and P. Tournoux. *Co-planar Stereotaxic Atlas of the Human Brain.* Thieme Medical Publisher Inc, New York, January 1988.

[13] G. Schaltenbrand and W. Wahren. *Atlas for Stereotaxy of the Human Brain.* Thieme, Stuttgart, 2nd edition, January 1977.

[14] D. L. Collins, A. P. Zijdenbos, V. Kollokian, J. G. Sled, N. J. Kabani, C. J. Holmes, and A. C. Evans. Design and construction of a realistic digital brain phantom. *IEEE Trans Med Imaging*, 17(3):463–468, Jun 1998.

[15] Joseph Stancanello, Pantaleo Romanelli, Nicola Modugno, Pietro Cerveri, Giancarlo Ferrigno, Fulvio Uggeri, and Giampaolo Cantore. Atlas-based identification of targets for functional radiosurgery. *Med Phys*, 33(6):1603–1611, Jun 2006.

[16] K. W. Finnis, Y. P. Starreveld, A. G. Parrent, A. F. Sadikot, and T. M. Peters. Three-dimensional database of subcortical electrophysiology for image-guided stereotactic functional neurosurgery. *IEEE Trans Med Imaging*, 22(1):93–104, Jan 2003.

[17] F. Javier Sánchez Castro, Claudio Pollo, Reto Meuli, Philippe Maeder, Meritxell Bach Cuadra, Olivier Cuisenaire, Jean-Guy Villemure, and Jean-Philippe Thiran. Cross validation of experts versus registration methods for target localization in deep brain stimulation. In *MICCAI*, pages 417–424, 2005.

[18] S. C. Deoni, B. K. Rutt, A. G. Parrent, and T. M. Peters. Segmentation of thalamic nuclei using a modified k-means clustering algorithm and high-resolution quantitative magnetic resonance imaging at 1.5 t. *Neuroimage*, 34(1):117–126, Jan 2007.

[19] T. Guo, Y. P. Starreveld, and T. M. Peters. Evaluation and validation methods for intersubject nonrigid 3D image registration of the human brain. In R. L. Galloway, Jr. and K. R. Cleary, editors, *Medical Imaging 2005: Visualization, Image-Guided Procedures, and Display. Edited by Galloway, Robert L., Jr.; Cleary, Kevin R. Proceedings of the SPIE, Volume 5744, pp. 594-603 (2005).*, pages 594–603, April 2005.

[20] F. Kruggel and Y. Cramon. Aligment of magnetic-resonance brain datasets with the stereotactical coordinate system. *Medical Image Analysis*, 2(3):175–185, 1995.

[21] W. L. Nowinski. Anatomical targeting in fnctional neurosurgery by the simultaneos use of multiple schaltenbrand-warhen brain atlas microseries. *Medical Image Analysis*, (71):103–116, 1998.

[22] T. F. Cootes, G. J. Edwards, and C. J. Taylor. A comparative evaluation of active appearance model algorithms. In John N. Carter and Mark S. Nixon, editors, *BMVC*. British Machine Vision Association, 1998.

[23] Timothy F. Cootes, C. Beeston, Gareth J. Edwards, and Christopher J. Taylor. A unified framework for atlas matching using active appearance models. In *IPMI*, pages 322–333, 1999.

[24] A. A. Nielsen. *Analysis of Regularly and Irregularly Sampled Spatial, Multivariate, and Multi-temporal Data*. PhD thesis, Informatics and Mathematical Modelling, Technical University of Denmark, Richard Petersens Plads, Building 321, DK-2800 Kongens Lyngby, Denmark, 1994.

[25] F. L. Bookstein. Principal warps: Thin-plate splines and the decomposition of deformations. *IEEE Transactions on Pattern Analysis and Machine Intelligence , June 1989*, PAMI-11(6):567–585, 1989.

[26] H. Wenland. Piecewise polynomial, positive definite and compactly supported radial functions of minimal degree. *Adv Comput Math*, 4:389, 1995.

[27] Mike Fornefett, Karl Rohr, and H. Siegfried Stiehl. Radial basis functions with compact support for elastic registration of medical images. *Image Vision Comput*, 19(1-2), 2001.

[28] B. S. Morse, T. S. Yoo, P. Rheingans, D. T. Chen, and K. R. Subramanian. Interpolating implicit surfaces from scattered surface data using compactly supported radial basis functions. In Bob Werner, editor, *Proceedings of the International Conference on Shape Modeling and Applications (SMI-01)*, pages 89–98, Los Alamitos, CA, May 7–11 2001. IEEE Computer Society.

[29] Z. Wu. Compactly supported positive definite radial basis functions. *Adv Comput Math*, 4:283, 1995.

[30] George, A. and Liu, J. W. H. *Computer Solution of Large Positive Definite Systems*. Prentice-Hall, 1981.

[31] E. Anderson, Z. Bai, C. Bischof, S. Blackford, J. Demmel, J. Dongarra, J. Du Croz, A. Greenbaum, S. Hammarling, A. McKenney, and D. Sorensen. *LAPACK Users' Guide*. Society for Industrial and Applied Mathematics, Philadelphia, PA, third edition, 1999.